Geophysical Prospecting, 2010, **58**, 541–548 doi: 10.1111/j.1365-2478.2009.00849.x

Reflection point sideslip and smear in imaging below dipping anisotropic media

Rob Vestrum[1]* and Don Lawton[2]

[1]*Thrust Belt Imaging, Data Processing, 2300, 645, 7 Avenue SW, Calgary, Alberta T2P 4G8, Canada, and* [2]*University of Calgary, Department of Geoscience, 844 Campus Place Northwest, Calgary, Alberta T2N 1N4, Canada*

Received June 2009, revision accepted October 2009

ABSTRACT

Dipping anisotropic clastic strata are ubiquitous in fold and thrust belts. Geological structures below these strata will be mispositioned laterally and vertically on seismic images if we do not properly correct for seismic anisotropy during migration. The magnitude of this lateral mispositioning of a target structure varies with source-receiver offset, so reflection points will be smeared in the final stacked image. Raytracing demonstrates the lateral-position and smear phenomena when imaging structures below tilted transversely isotropic media. Analysis of the raytracing results predicts the quantity of lateral-position error and reflection-point smear on a seismic image. We created numerical-model seismic data to show reflection-point smear on synthetic seismic images and to evaluate the accuracy of the predictions from raytracing.

INTRODUCTION

Sideslip error refers to the lateral mispositioning of structures below dipping anisotropic strata on seismic images when seismic velocity anisotropy is ignored in the migration algorithm. Several authors have proposed solutions to the lateral-position problem in terms of anisotropic depth migration that incorporates tilted transverse isotropy (TTI) symmetry (e.g., Ball 1995; Vestrum and Muenzer 1997; Ferguson and Margrave 1998; Vestrum, Lawton and Schmid 1999). Anisotropic depth migration has now become common in hydrocarbon exploration in thrust-belt environments and we attempt here to understand more fully the imaging effects corrected by anisotropic migrations, yielding improved images. By isolating the anisotropic imaging effects from other complex wave-propagation effects, this study investigates how the mispositioning of structures changes with source-receiver offset and how this offset variation affects the seismic image.

For the purposes of this study, we consider imaging structures below weak transversely isotropic strata with a tilted axis of symmetry. Thomsen (1986) provided a convenient expression for the phase velocity magnitude, v, as it varies with direction in terms of angle from the symmetry axis, θ, and elastic constants, ε and δ:

$$v(\theta) = v_0(1 + \delta \sin^2\theta \cos^2\theta + \varepsilon \sin^4\theta). \quad (1)$$

Figure 1 illustrates a wavefront propagating in a TTI medium. The phase velocity, $\vec{v}$, is the velocity of the wave normal to the wavefront. The sideslip velocity $\vec{s}$, is the velocity of wave motion in the direction tangential to the wavefront. Vector addition of sideslip-velocity and phase-velocity vectors yields the group velocity, $\vec{g}$, which is the velocity of energy transport (for a detailed discussion on the relationship between group and phase velocity in anisotropic media, please refer to Appendix B of Dellinger (1991)). We obtain the equation for the sideslip velocity magnitude, s, by differentiating equation (1) with respect to δ:

$$s \equiv \frac{\partial v}{\partial \theta} = v_0[2\delta(\cos^3\theta \sin\theta - \cos\theta \sin^3\theta) + 4\varepsilon \cos\theta \sin^3\theta]. \quad (2)$$

The sideslip distance, S, as defined by Vestrum *et al.* (1999), is the horizontal displacement of a reflection point

*E-mail: rob@tbi.ca

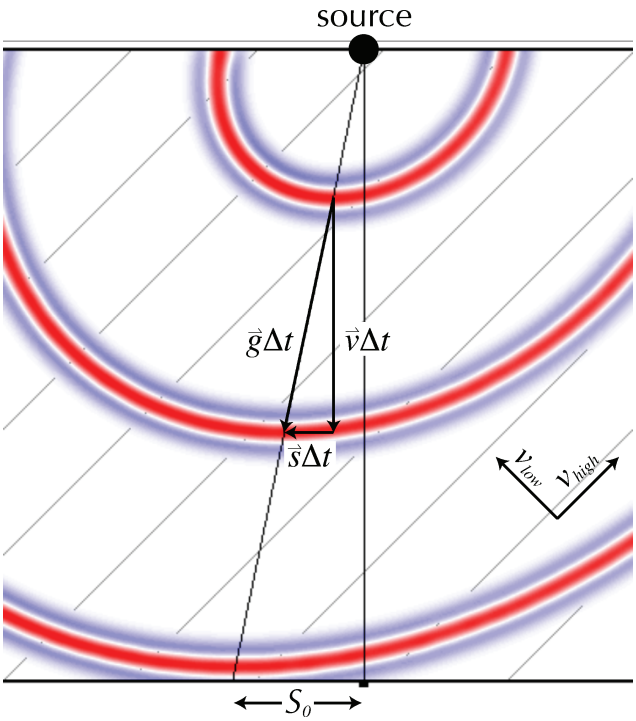

Figure 1 Waves propagating across dipping anisotropic strata separated by Δt. The grey diagonal lines represent the 45° dip orientation. The lateral distance between the source location and the zero-offset reflection point is defined as the zero-offset sideslip distance S_0.

from the midpoint between seismic source and receiver for a horizontal reflector below a layer of anisotropic strata with a tilted axis of symmetry. If we consider only the zero-offset sideslip distance as a function of the vertical thickness of the dipping anisotropic overburden, ΔZ, and the magnitudes of the sideslip velocity, s, and phase velocity, v, we define the zero-offset sideslip distance, S_0, as:

$$S_0 \equiv \frac{s}{v}\Delta Z. \tag{3}$$

Since this equation is valid only in the case of zero-offset distance between the source and receiver, two questions we address here are: 1) how does the sideslip distance, S, change with source-receiver-offset? and 2) how does the variation of S with source-receiver offset affect the quality of the final seismic image?

RAYTRACE MODELLING

To answer the first of the two questions posed above, raytracing was undertaken through a simple TTI velocity model to determine the lateral position of the minimum-traveltime reflection point for each source-receiver offset. The velocity model is simply a horizontal reflector at the base of a homogeneous dipping anisotropic layer, 2000 m in vertical thickness, with an axis of symmetry tilted at 15° from the vertical. The anisotropic parameters used for the overburden in these tests were chosen to be $\varepsilon = 0.12$ and $\delta = 0.03$, which are commonly used values in thrust-belt anisotropic depth migration (e.g., Vestrum 2002; Gittins, Vestrum and Gillcrist 2004). Figure 2 shows minimum-traveltime raypaths for offsets ranging from 0–4000 metres for this model. Not only is the reflection point shifted laterally from the midpoint between source and receiver but also each offset images a slightly different location in the subsurface. Here, the lateral shift from the midpoint of the reflection point for the 4000 m offset is 263 m, which is much larger than the zero-offset sideslip distance (48 m) predicted from equation (3). We define the distance from the reflection point at zero-offset to the reflection point at the maximum offset as the 'reflection-point smear', S' (Fig. 2), because all of the traces that share this common midpoint are not imaging the same point on the reflector.

Figure 3 shows graphs of reflection-point smear (S') and average sideslip distance ($\bar{S}$) over dip angles ranging from 0–90° for anisotropic parameters $\varepsilon = 0.12$ and $\delta = 0.03$. In this example, the maximum offset is equal to twice the reflector depth, as in Fig. 2, and both smear and sideslip are normalized by the reflector depth. The value for the average sideslip is defined simply as the distance to the point halfway between the zero-offset sideslip distance and the far-offset sideslip distance. As a sample calculation, if the overburden dip is 15°, then the smear-to-depth ratio is 0.110 and the sideslip-to-depth ratio is 0.077. Thus, if the anisotropic overburden is 1 km thick, then we predict a sideslip distance of 77 m and a reflection-point smear of 110 m, which one could consider in terms of a lateral-position error of 77 ± 55 m.

Figure 3 also shows that smear and sideslip are similar in maximum absolute magnitude. This offset dependence of the lateral-position error can be as much a seismic-imaging pitfall as the side slip induced lateral-position error itself. We would thus expect better focused depth-migrated seismic images if we correct for velocity anisotropy, including both sideslip and smear.

If the maximum offset equals the depth to the reflector, the sideslip and smear dependency on dip is illustrated in Fig. 4. In this case, with a smaller offset-to-depth ratio, the maximum magnitude of sideslip is similar to that shown in Fig. 3 but the maximum magnitude of smear is reduced. In particular, the significant sideslip and smear at the shallower overburden dips that we observe in Fig. 3 are reduced on the limited-offset case shown in Fig. 4.

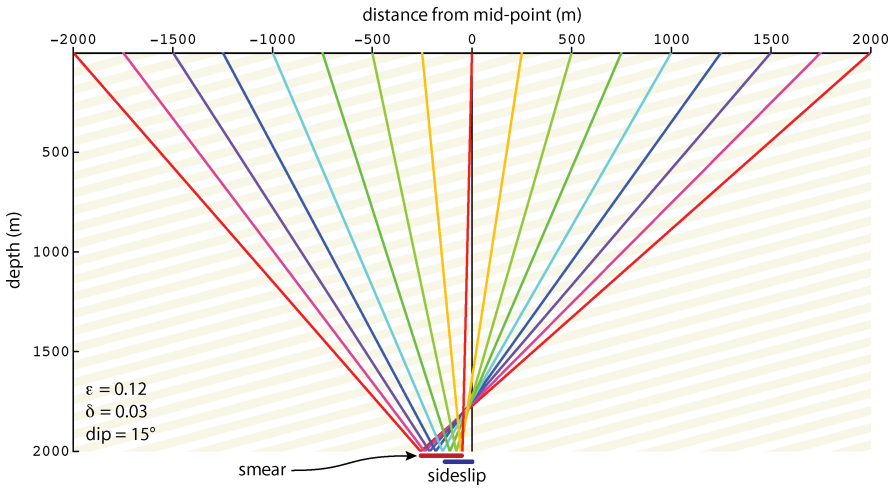

Figure 2 Rays with common mid-point illustrating lateral shift of reflection point with offset for a horizontal reflector beneath anisotropic strata dipping at 15°.

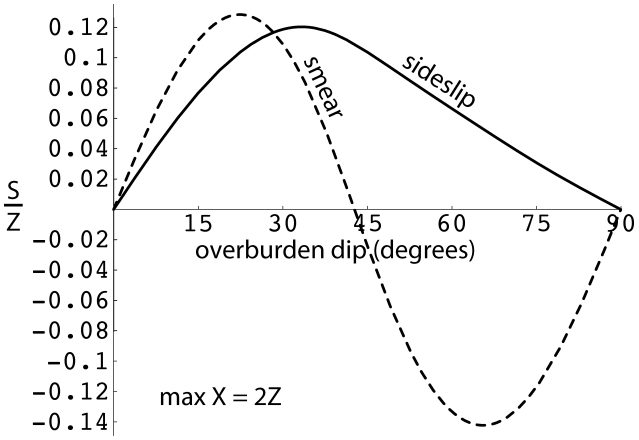

Figure 3 Reflection-point smear and average sideslip versus overburden dip for maximum offset equal to twice the depth of the reflector.

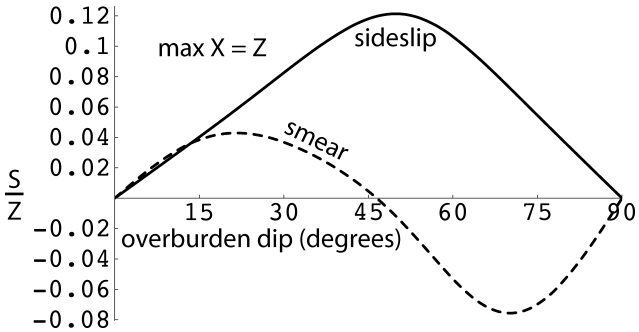

Figure 4 Reflection-point smear and average sideslip versus overburden dip for maximum offset equal to the depth of the reflector.

NUMERICAL MODELLING

After examining the behaviour of the sideslip distance with respect to source-receiver offset and how that changes with reflector dip, we now consider how the offset dependency of sideslip distance affects the quality of the seismic image. This was done by undertaking prestack depth migration of numerical data generated using SU modelling codes (Alkhalifah 1995).

The model used is a horizontal reflector with a sharp edge that is buried within a homogeneous TTI medium (Fig. 5). Four models were tested with this same geometry and varying only the dip of the TTI background medium. The dips of the anisotropic strata in the four models were: 0°, 15°, 30°

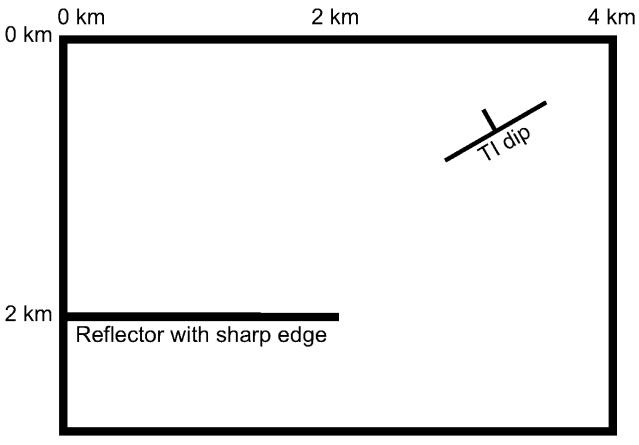

Figure 5 Diagram of TTI velocity model used in the modelling study.

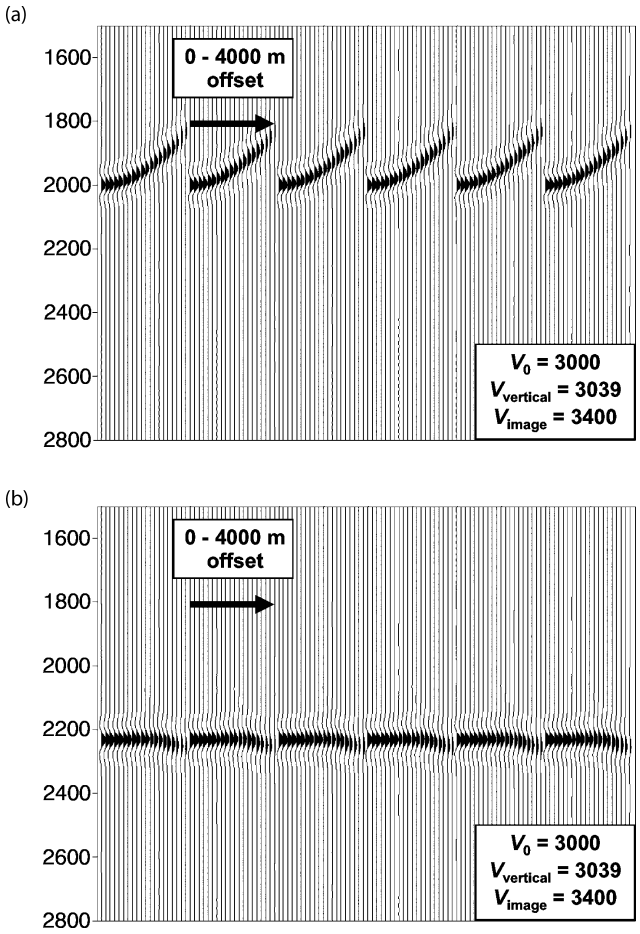

Figure 6 Image-gather analysis of model data migrated ignoring the anisotropy. a) Migrated image gathers that result from migrating with the vertical velocity, $v_{vertical}$. b) Migrated image gathers that result from migrating with an optimum imaging velocity that produces nearly flat gathers, v_{image}.

and 45°. The purpose of the modelling was to observe the consequences of ignoring anisotropy in the seismic-imaging process. To achieve this result, we chose the isotropic migration velocity for each numerical-model data set that yielded the best image possible using isotropic migrations. The resulting images are thus isotropic depth migrations of anisotropic forward-model data.

IMAGE-GATHER ANALYSIS

Since our goal is a well-focused seismic image, we used the depth-migration velocity that best flattened the image gathers, sacrificing the accuracy of reflector depth. Figure 6(a) shows the image gathers from a prestack depth migration using the true vertical velocity. The near offset is imaged at the correct model depth but as offset increases, the traveltime is reduced because of the anisotropy, resulting in far offset traces that image the reflector at a lesser depth than that predicted by the isotropic depth migration. Figure 6(b) shows the image gathers for an isotropic imaging velocity of 3400 m/s, which is the velocity that yields image gathers that exhibit minimal residual moveout. In this case, the depth of the imaged reflector is greater than the true depth in the model, which is a common problem observed with isotropic depth migrations (e.g., Schultz and Canales 1997).

In the process of inspecting the image gathers for the various models, we made several additional interesting observations. Figure 7 shows migrated image gathers from the four forward models. In the vertical transverse isotropy (VTI) case (Fig. 7a), where the dip of the anisotropic background medium is 0°, we observed the typical negative residual moveout on the far offset traces as described by Alkhalifah (1997) when we ignore the seismic anisotropy. In industry practice, the upturned shape of the reflector on the far offsets is commonly referred to as a 'hockey stick'. The 15° case (Fig. 7b) shows more depth error than the 0° case but the residual moveout is reduced. The largest depth error is in the 30° case (Fig. 7c) and at this dip, the residual moveout on the longest offsets shows a slightly down-turned shape. For the steepest dip in this study, 45°, shown in Fig. 7(d), the depth error is reduced as the vertical velocity increases. The longest offsets now show negative residual moveout resulting in a down-turned orientation of the hockey-stick shape.

From the image-gather analysis discussed above, we observed that the shape of the residual moveout of a reflection changes depending on the dip of the overlying anisotropic medium. One may conclude that when strata above the imaging target has non-zero dip, the presence or absence of hockey-stick shaped residual moveout on image gathers is not a unique indicator of the presence or absence of seismic anisotropy in the overburden.

MIGRATED-STACK ANALYSIS

The ultimate goal of this work is to observe the seismic imaging effects on a migrated, stacked seismic section, as it is the process of stacking over a range of migrated source-receiver offsets that yields reflection point smear if isotropic velocities are assumed through anisotropic layers. Figure 8 shows partial stacks of near (Fig. 8a), mid (Fig. 8b) and far (Fig. 8c) offsets. The offset ranges are 0–1300 m for the near offsets, 1300–2600 m for the mid-offsets and 2600–4000 m for the far offsets; the reflector depth is 2000 m. On each seismic image in

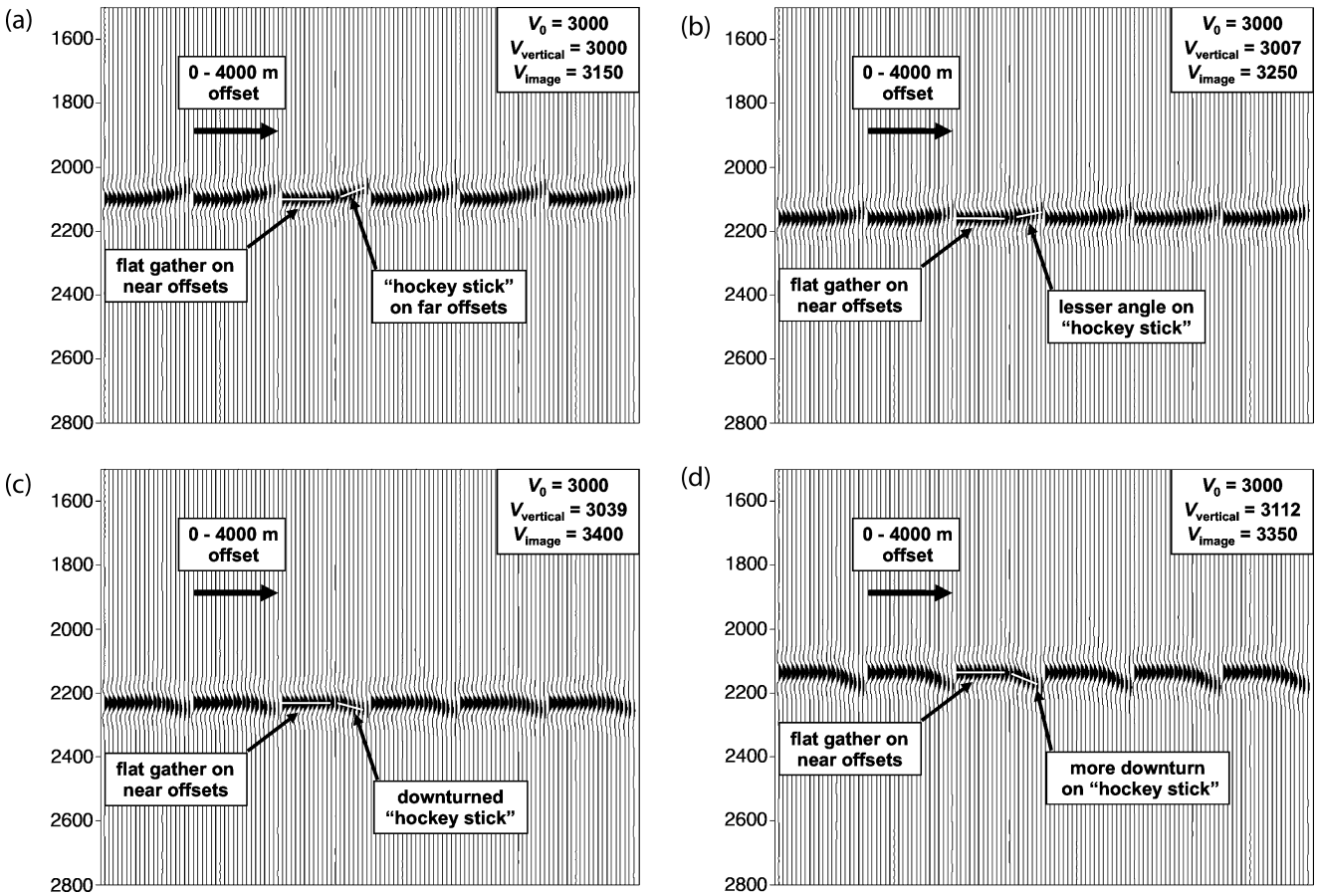

Figure 7 Isotropically migrated image gathers from the four models: a) 0° dip or VTI, b) 15° dip, c) 30° dip, d) 45° dip. v_0 is the model velocity normal to bedding, $v_{vertical}$ is the vertical model velocity and v_{image} is the velocity used to flatten the near offsets on the image gathers.

Fig. 8, the interpreted end of the reflector is marked with three vertical lines, each one corresponding with one of the three offset ranges, as labelled. The horizontal line on each image represents the true location of the model reflector. Using these markers, we can compare the lateral position of the edge of the reflector image as its position changes with offset. Note that the lateral-position error—the horizontal distance between the reflector position and the imaged position—increases as offset increases. The full offset stack in a final depth-migrated section will result in blurring of the end of the imaged reflector.

The final full-offset migrated images from the four models (Fig. 9) show varying degrees of lateral-position error and reflection-point smear at the edge of the reflector.

Figure 9(a) shows the result that we would expect from a seismic migration that accurately corrects for all wave-propagation effects, including anisotropy. The horizontal line represents the true location of model reflector overlaid on the seismic image that results from migrating with the model parameters from the known forward model. The seismic image shows an accurate depth of the reflector and a reasonably sharp edge. The spacing of these seismic traces is 10 m, so the uncertainty in the position of the edge of that reflector is approximately 20 m or 1% of the depth to the reflector.

In the VTI case (Fig. 9b), the imaged reflector is deeper than the true model depth. Although the sideslip and smear equations predict no lateral-position error or reflection-point smear in the VTI case, the edge of the reflector in Fig. 9(b) appears poorly focused over distances of tens of metres when compared with the imaged reflector in Fig. 9(a). This blurring of the edge of the reflector is caused by the inaccuracy of the diffraction curvature when migrating the seismic data ignoring anisotropy. In the offset domain (Fig. 7) there is residual moveout on the far offsets when isotropy is assumed and a similar error occurs in the migration-operator domain as the algorithm works to correct for the energy that scatters from the edge of the reflector. One may conclude from

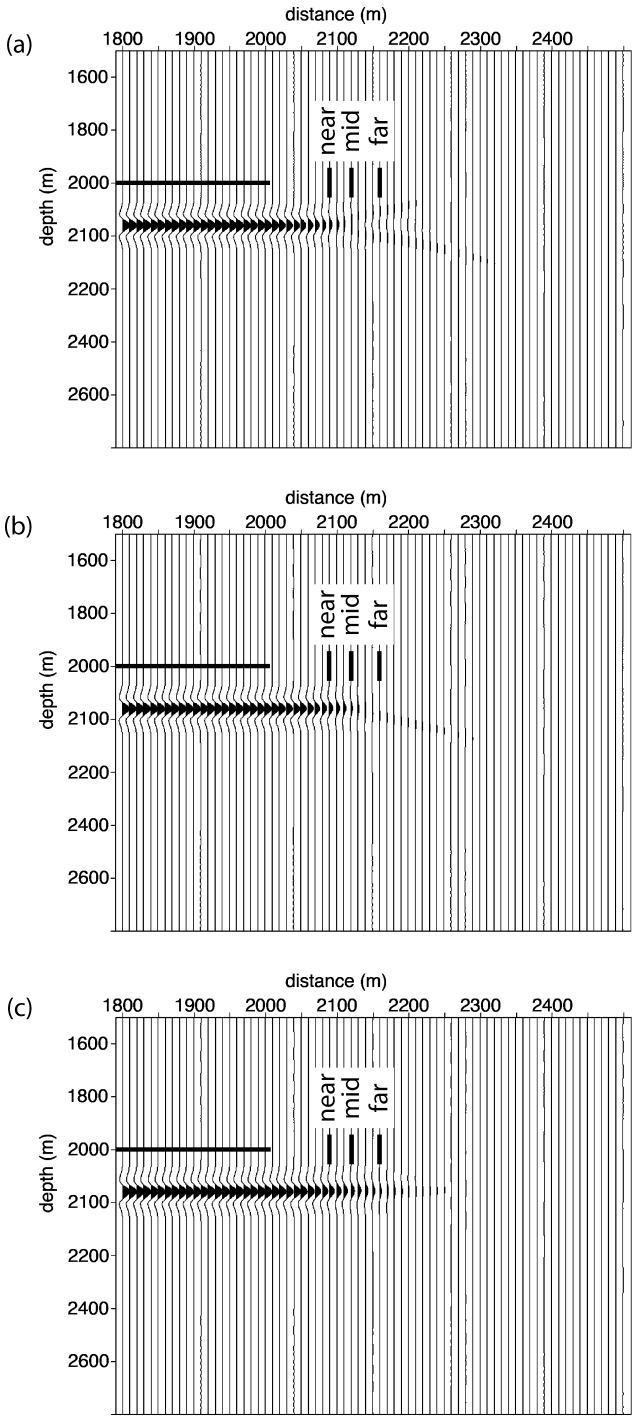

Figure 8 Isotropically migrated stacks of limited-offset ranges from the 15° model data: a) near offsets from 0–1300 m, b) mid offsets from 1300–2600 m, c) far offsets from 2600–4500 m. Green marker indicates estimate of reflector edge on the near offset, blue for the mid-offset and orange for the far offset. Trace increment is 10 m.

both image-gather and stack analyses that there will be loss in focusing in the VTI case if anisotropy is ignored in the migration, even when there are no sideslip and smear effects present.

In the TTI cases (Fig. 9c–e), the lateral-position error increases with dip of the anisotopic overburden, over the tested range from 15–45°. The 15° dipping model (Fig. 9c) and the 30°dipping model (Fig. 9d) show more smear or blurring of the reflector edge than is seen in the 45° dipping case (Fig. 9e). This observation is consistent with the predicted maximum sideslip shown in Fig. 3, where the maximum smear is in the range of 15–30° overburden dip and the reflection-point smear is near zero at 45° overburden dip.

The evaluation of results from the numerical models shows that raytracing predicted the lateral-position error accurately but overestimated the smear. In the 15° dip example, the raytracing results (Fig. 3) predicted a sideslip error of 150 m and a smear of 230 m. Figure 10 shows the seismic image of the 15° TTI model data with identifiers to show the sideslip and an estimate of the smear of the imaged reflector. Given the uncertainty in estimating the smearing of the reflector, it is difficult to quantify the accuracy of the predicted sideslip.

In a real-world case of seismic imaging in the presence of noise, these data suggest that the smear of the seismic reflector will be approximately half of what is predicted by raytracing.

DISCUSSION AND CONCLUSIONS

Exploration seismic data are more complex than the simple homogeneous TTI models in this study. The results of this numerical study show how dipping anisotropy, in isolation, affects the seismic imaging of subsurface reflectors. Correcting for anisotropy in seismic imaging is simply one component of a larger portfolio of major imaging issues including velocity heterogeneity and near-surface effects. The modelling of the TTI imaging effects in isolation demonstrates the pitfalls of ignoring seismic anisotropy in depth imaging.

Smear and sideslip blur and misposition reflectors below dipping anisotropic strata when isotropic velocities are assumed in the depth-migration velocity model. They are two imaging effects that are corrected with the application of anisotropic depth migration that accurately handles TTI media. Observations from numerical-model seismic data showed approximately half of the reflector smear than was predicted by the raytracing. The important points of this study may be summarized as:

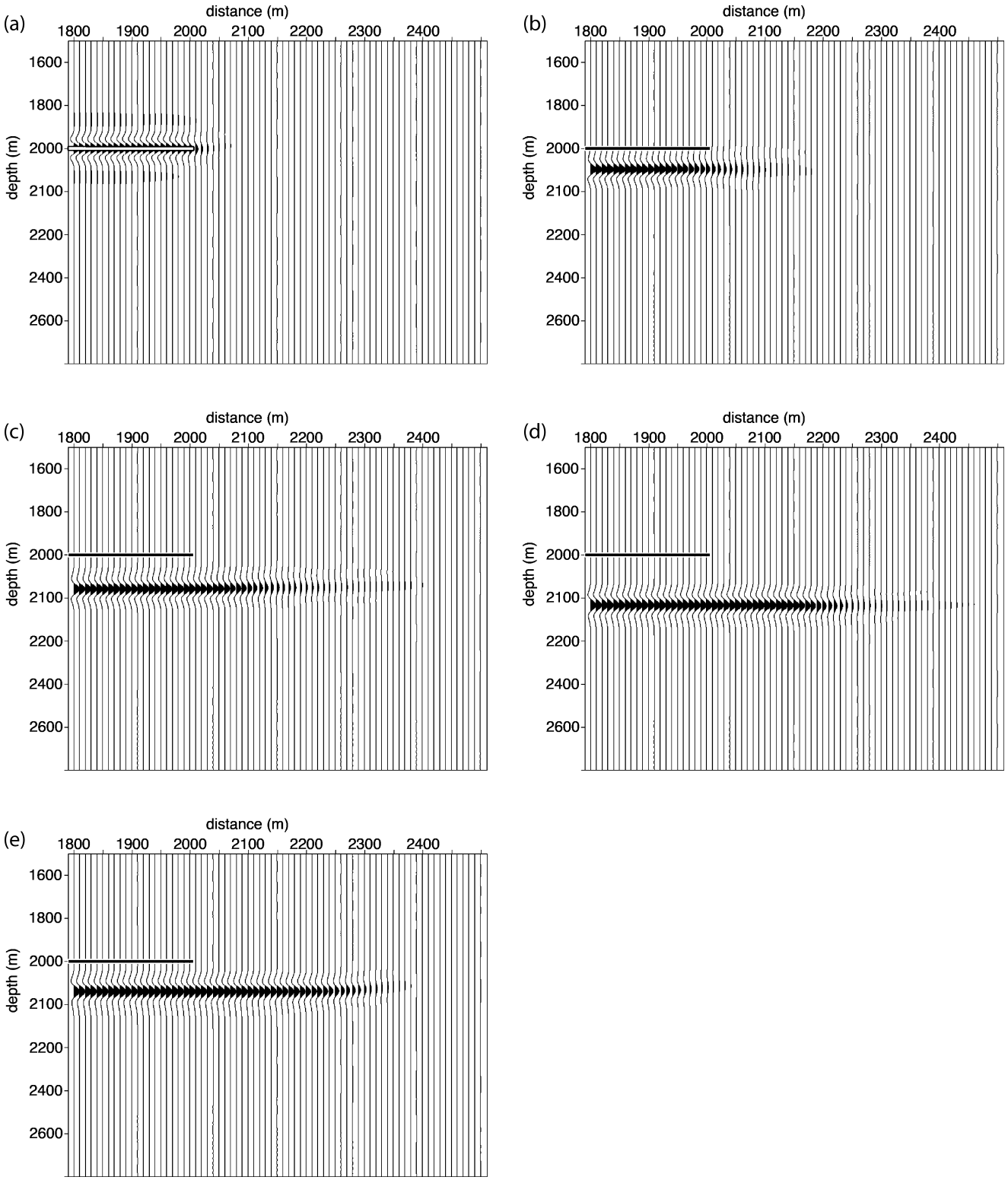

Figure 9 Final isotropic depth migrated stacks of all offsets. The red line indicates the position of the model reflector. a) Isotropic forward model, b) VTI forward model, c) 15° dipping TTI forward model, d) 30° dipping TTI forward model and e) 45° dipping TTI forward model.

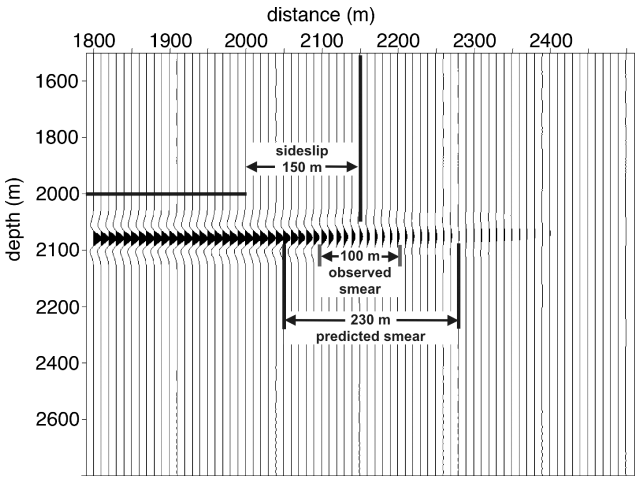

Figure 10 Measurements of observed and predicted sideslip and smear for 15° dipping TTI model.

- sideslip of seismic waves causes lateral-position errors on seismic images, with the largest lateral-position problem in overburden-dip range 20°–50°;
- offset-dependency of the lateral-position error causes reflection-point smear on seismic images, with the largest smear problem in the overburden-dip range of 10°–35°.

ACKNOWLEDGEMENTS

The authors wish to acknowledge the sponsors of the Fold/Fault Research Project at the University of Calgary for their support of this research. Thanks also to Thrust Belt Imaging for support and permission to publish this project.

REFERENCES

Alkhalifah T. 1995. Efficient synthetic-seismogram generation in transversely isotropic, inhomogeneous media. *Geophysics* **60**, 1139–1150.

Alkhalifah T. 1997. Velocity analysis using nonhyperbolic moveout in transversely isotropic media. *Geophysics* **62**, 1839–1854.

Ball G. 1995. Estimation of anisotropy and anisotropic 3-D prestack depth migration, offshore Zaire. *Geophysics* **60**, 1495–1513.

Dellinger J. 1991. *Anisotropic seismic wave propagation*. PhD thesis, Stanford University.

Ferguson R.J. and Margrave G.F. 1998. Depth migration in transversely isotropic media by nonstationary phase shift. 68th SEG meeting, New Orleans, Louisiana, USA, Expanded Abstracts, 1831–1834.

Gittins J., Vestrum R.W. and Gillcrist R. 2004. Overcoming thrust-belt imaging problems in Magdalena Valley, Colombia. 74th SEG meeting, Denver, Colorado, USA, Expanded Abstracts, 2021.

Schultz P. and Canales L. 1997. Seismic velocity model building: CE in Dallas, 2 November. *The Leading Edge* **16**, 1063–1064.

Thomsen L. 1986. Weak elastic anisotropy. *Geophysics* **51**, 1954–1966.

Vestrum R.W. 2002. 2D and 3D anisotropic depth migration case histories. 72nd SEG meeting, Salt Lake City, Utah, USA, Expanded Abstracts.

Vestrum R.W., Lawton D.C. and Schmid R.S. 1999. Imaging structures below dipping TI media. *Geophysics* **64**, 1239–1246.

Vestrum R.W. and Muenzer K. 1997. Anisotropic depth imaging below dipping shales. CSEG 1997 National Meeting.